Accepted Manuscript

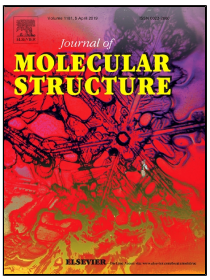

Modulation of magnetism and Study of impedance and alternating current conductivity of $Zn_{0.4}Ni_{0.6}Fe_2O_4$ spinel ferrite

S.B. Amor, A. Benali, M. Bejar, E. Dhahri, K. Khirouni, M.A. Valente, M.P.F. Graça, F. Al-Turjman, J. Rodriguez, A. Radwan

PII:	S0022-2860(19)30183-8
DOI:	10.1016/j.molstruc.2019.02.053
Reference:	MOLSTR 26210
To appear in:	*Journal of Molecular Structure*
Received Date:	10 October 2018
Accepted Date:	13 February 2019

Please cite this article as: S.B. Amor, A. Benali, M. Bejar, E. Dhahri, K. Khirouni, M.A. Valente, M.P. F. Graça, F. Al-Turjman, J. Rodriguez, A. Radwan, Modulation of magnetism and Study of impedance and alternating current conductivity of $Zn_{0.4}Ni_{0.6}Fe_2O_4$ spinel ferrite, *Journal of Molecular Structure* (2019), doi: 10.1016/j.molstruc.2019.02.053

Graphical abstract

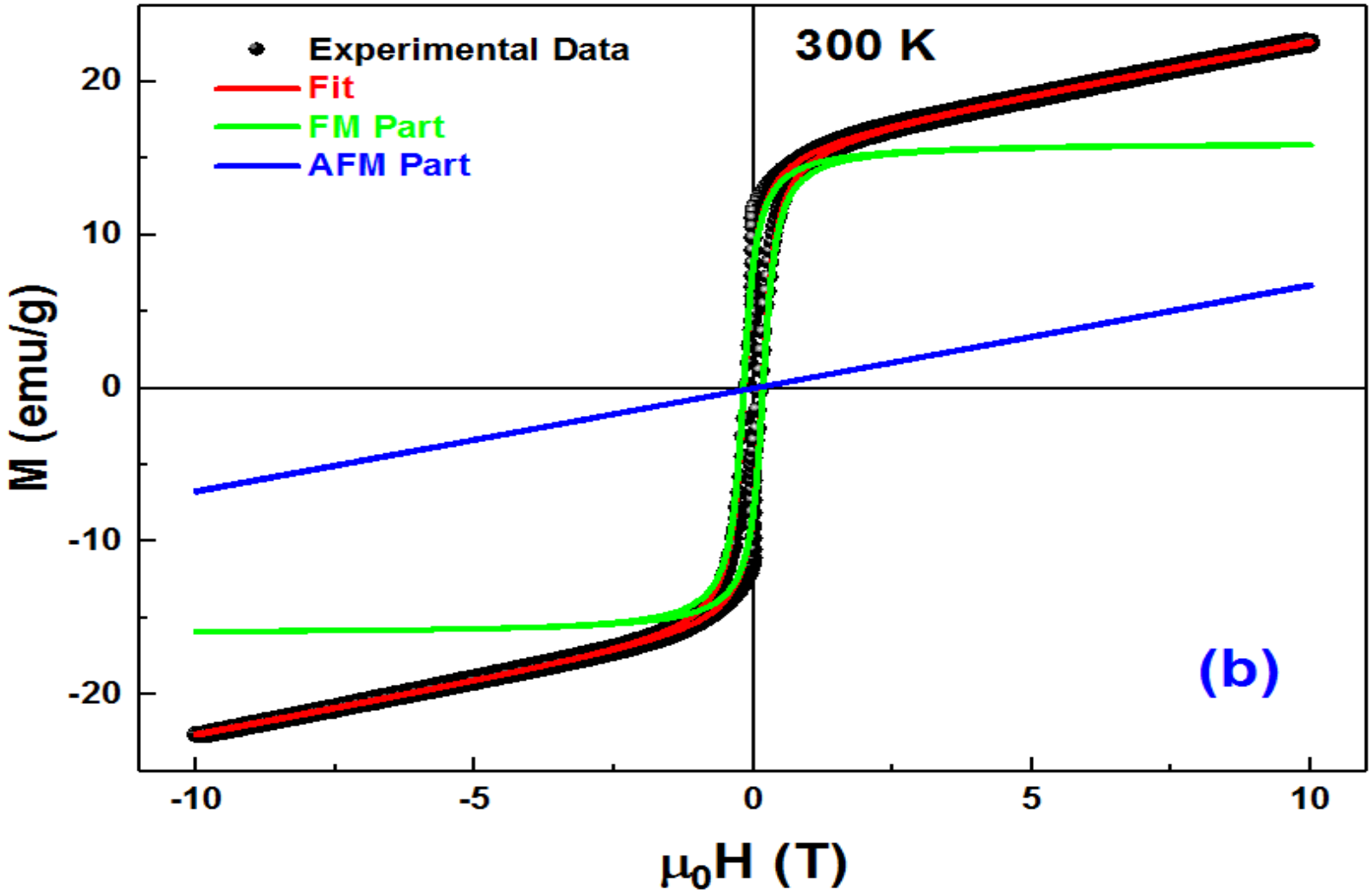

Modulation of magnetism and Study of impedance and alternating current conductivity of $Zn_{0.4}Ni_{0.6}Fe_2O_4$ spinel ferrite

S. B. Amor[a] , A. Benali [a,e,c], M. Bejar[a], E. Dhahri[a], K. Khirouni [b], M.A. Valente [c], M.P.F. Graça [c],F. Al-Turjman [d], J. Rodriguez [e], A. Radwan [e]*

[a] *Laboratoire de Physique Appliquée, Faculté des Sciences, B.P. 1171, 3000 Sfax, Université de Sfax, Tunisia.*
[b] *Laboratoire de Physique des Matériaux et des Nanomatériaux Appliquée à l'Environnement, Faculté des Sciences de Gabes Cite Erriadh, Université de Gabes, 6079 Gabes, Tunisia.*
[c] *I3N, Physics Department, University of Aveiro, Campus de Santiago, Aveiro, Portugal.*
[d] *Computer Engineering Dept., Middle East Technical University, N. Cyprus Campus, 99738, Mersin 10, Turkey.*
[e] *Instituto de Telecomunicações – Aveiro, Campus Universitário de Santiago, 3810-193, Aveiro, Portugal.*

Abstract

A spinel ferrite sample $Zn_{0.4}Ni_{0.6}Fe_2O_4$ was prepared by a conventional solid-state reaction method, at high temperature. This compound was found to exhibit a single phase and crystallize in a cubic structure with Pm3m Space group. The complex impedance was investigated in the temperature range 400–700 K and in the frequency range 100 Hz - 1 MHz. The Z-impedance analysis revealed that the relaxation phenomenon is strongly dependent on temperature and frequency. The impedance plane plot showed semi-circle arcs at different temperatures, and a proposed electrical equivalent circuit explained its results. The temperature and frequency dependence of the ac conductivity was shown to obey the universal Jonscher's power law. The activation energy, inferred from the impedance spectrum, was confirmed to match very well with those estimated from the conduction mechanism, indicating that the relaxation process and conductivity have the same origin. The magnetization is due to the ferromagnetic interactions between iron ions.

Keywords*: Spinel, Solid state, relaxation, conduction mechanism*, *Modulation*.

I. INTRODUCTION

Ni-Zn ferrites are soft ferromagnetic materials, which in high-frequency operation have high resistivity values, small eddy current losses and low magnetic coercivity [1]. These materials have always been of great interest, thanks to their technological applications namely at high frequencies [1, 2], where the eddy current losses have to be low. It is important to note that many methods could have been used to synthesize these ferrites such as ceramic [3], co-precipitation [4], combustion [2], precursor [5], hydrothermal method [6, 7], Micelle (MIC) route [7]… etc. The most known disadvantages of these methods are high reaction temperatures, prolonged reaction time, complicated procedure and especially the use of reducing agents that upset the environment and slightly modified the properties.

On the one hand, the properties of ferrites are sensitive to their composition and microstructure, which in turn are strongly dependent upon the processing method used to synthesize them [8]. On the other hand, they are dependent on the measuring temperature, magnetic or electric field applied and the frequency of the signal. Furthermore, ferrites have excellent magnetic properties and a high electrical resistance, which make them excellent core material for recording heads loading coils [9], power transformers in electronics [10], antenna rods [11], microwave devices and telecommunication applications [1], anode material in Li-ion batteries [12], piezoelectric actuators and transducers [13].

The magnetic and the structural properties of this type of materials have been broadly studied [14-20], but ~~there are~~ few reports are available on Impedance spectroscopy of the Ni–Zn ferrites [21, 22]. ~~Moreover, impedance spectroscopy is a valuable technique~~ Obviously, this technique is highly appropriate for the characterization of inhomogeneous electrical materials, ~~which uses~~ relying on the different frequency

dependencies of the constituent components for their separation. The responses of all components, such as grain boundary and bulk impedances in electronic ceramics, take the form of electrical relaxations and can be modeled using simple RC parallel circuit elements. Each electric component has its own characteristic relaxation time, given by the magnitude of the RC product, which could be separated in the frequency domain **[23].**

It was reported previously that the $Ni_{0.6}Zn_{0.4}Fe_2O_4$ compound prepared with the ceramic method with ~~using~~ the 5%-Polyvinyl alcohol as a binder, crystallized in the cubic structure and the lattice parameter was found to be equal to 8.35 Å **[21]**. The Nyquist plots (Z" vs Z') showed two semicircles according to the grain and the grain boundary contributions. These two contributions were also seen in the $Ni_{1-x}Zn_xF_{e2}O_4$ samples ~~which have been~~ prepared with the combustion method **[24]**.

In the present paper, Ni-Zn ferrites were prepared by the conventional solid-state reaction method, at high temperature, and without any binder. XRD was used to characterize synthesized material and then alternating current (ac) impedance spectroscopy was used to study the effects of temperature and frequency on the Ni-Zn compound.

II. Experimental Details

The solid-state route was used to prepare the $Zn_{0.4}Ni_{0.6}Fe_2O_4$ Spinel Ferrite ceramic (ZNFO). A stoichiometric mixture of Fe_2O_3, ZnO and NiO powder oxides with a purity of 99.99% was ground and pressed using a uniaxial pressure system under 105 N/cm^2 pressure into 10 mm diameter pellets. The pellets were submitted to heat treatments at different temperatures (800, 900, 1000 and 1200 °C), for 24 h.

III. RESULTS AND DISCUSSIONS

1) XRD study:

Figure 1 depicts the XRD pattern of the prepared ZNFO compound. One can see clearly sharp and intensive peaks indicating the good crystallization of the synthesized compound. Using the X'Pert Highscore software, and according to the diffractions peaks in the XRD data that matched well with those of the pure $ZnFe_2O_4$ we confirm the formation of a pure cubic structure without any impurity. The Rietveld refinements of the XRD data performed using Fullprof program **[25]** revealed that this compound crystallized in the cubic structure, with the *Pm3m* space group in which the refined lattice parameters (a = b = c) and the volume (V) were found to be, respectively, equal to 8.3712 **Å** and 586.631 **Å³**. These values are slightly smaller than those previously reported **[21]**.

The Scherrer formula **[26]** was used to calculate the average crystallite size (D_{SC}) based on the full-width at half maximum (β) of the most intense peak and its Bragg angle (θ) as mentioned in the following equation:

$$D_{SC} = \frac{0.9 \times \lambda}{\beta \cos\theta}$$

where λ is the used wavelength ($\lambda_{Cu\text{-}K\alpha 1}$ = 1.5406). The D_{SC} value of our sample is about 72 nm which confirm the nanoscale nature of the ZNFO compound.

Figure 2 (a) shows a typical TEM spectrum of the $Zn_{0.4}Ni_{0.6}Fe_2O_4$ ceramic. This spectrum proves the existence of a non-uniformly distributed grains with an irregular morphology (spherical, ~~cube~~ cubic, polygonal). The particle size distribution was calculated from ≈140 nanoparticles randomly selected from the TEM micrograph by using the Image-J software. The results are expressed in **Figure 2 (b)** as grain number

(counts) *vs.* particle size (nm). These particles were distributed, for the $Zn_{0.4}Ni_{0.6}Fe_2O_4$ sample, according to a Lorentzian law (Blue solid line in **Figure 2 (b)**). The average particle size, generally known as grain, was of ~~(~~197 (± 5) nm greater than the average crystallite size of value ~ 72 nm determined by XRD. Considering that several crystallites could form each particle observed by SEM, the difference between the crystallite and the particle sizes becomes reasonable.

2) Impedance spectroscopy:

Figure 3 shows the frequency dependence of the real part (resistive) of impedance Z' for the studied compound at selected temperatures. When increasing the frequency, the magnitude of Z' firstly decreases up to a certain value to become frequency independent beyond this value. At low frequencies, the high amplitude of Z' decreases when increasing the temperature which applies an increase in the ac-conductivity as it ~~known~~ is common in dielectric materials **[27]**. The release of space charge implies the merge of the impedance real part (Z') values at high frequencies which is a direct result of the reduction of barrier properties of the material at higher temperatures **[28]**.

At the selected temperature, the effect of the frequency on the imaginary part of the complex impedance is shown in **Figure 4 (a)**. It can be seen the appearance of three peaks corresponding to three different specific frequencies (Known as the relaxation frequencies); which confirms that, in the studied compound, ~~it~~ there exist three different relaxation types, ~~and that~~ each ~~one is~~ being attributed to one of the three contributions mentioned before (grain, boundary grain and interfacial). ~~It is also noted that~~ Moreover, with increasing temperature, all Z" peaks were found to shift towards a higher frequency. These observations support the previous results to confirm the semi-conductivity behavior of the suggested sample and to prove the implication of charge carriers in the relaxation phenomenon and their thermal activation **[29]**.

On the other hand, for all peaks, the decrease of the values of Z''_{max} with the increase in temperature could be explained by the decrease in the resistance of materials [30]. Furthermore, the coalescing of all of these curves at higher frequencies (over 10^7 Hz) mimics the reduction of space charge polarization with the increase in frequency [31]. To calculate the activation energies, we use the Arrhenius law. The variation of relaxation frequency (f_{max}) with temperature can be expressed by Eq. (1) [32]:

$$f_{\max} = f_0 \exp\left(\frac{E_a}{k_B T}\right) \quad (1)$$

where f_0 is the relaxation frequency for high temperature, E_a is the activation energy for the relaxation process and k_B presents the Boltzmann constant. The logarithmic representation of the deduced f_{max} values is plotted against the inverse of temperature in Figure 4(b), using the Arrhenius model. This figure shows clearly the increase of the relaxation frequencies with the increase in temperature. The obtained values of activation energies are about 0.133 eV, 0.204 eV and 0.138 eV for grain, boundary grain and electrode contributions, respectively. These values are quite close to those earlier found in the literature [33-35].

Moreover, the complex impedance spectra (-Z" versus Z') of the synthesized ferrite $Zn_{0.4}Ni_{0.6}Fe_2O_4$ at different temperatures are presented in Figure 5. These plots are characterized by three semicircular arcs that are not centered on the real axis. The decentralization is indicative of a non-Debye type relaxation process and the material was found to obey the Cole-Cole formalism [36-38]. Every semicircle could be attributed to one of three contributions. At low frequencies, the semicircle can be attributed to the electrode contribution; at intermediate frequency range, the relaxation is due to the grain boundary contribution; while at high frequency, the semicircle is attributed to grain contribution.

The inset in **Figure 5** shows the Simulate Nyquist plots with the equivalent circuit elements for $Zn_{0,4}Ni_{0,6}Fe_2O_4$ at several temperatures. This circuit is modeled by a combination series of three parallel R-CPE circuits, with R as resistance and CPE the complex element; a constant phase element (capacity of the fractal interface). Let (R_1, R_2, R_3) and (CPE_1, CPE_2, CPE_3) be the resistance and capacitance of grains, grain boundaries, and electrodes, respectively, the CPE impedance (Z_{CPE}) is given by the following relation **[39, 40]**:

$$Z_{CPE} = \left[Q(j\omega)^{\alpha} \right]^{-1} \quad \textbf{(2)}$$

where *Q* is a proportional factor, ω is the angular frequency, and α is an empirical exponent close to 1. Depending on the value of the exponent α, the CPE has a behavior similar to the components conventionally used in equivalent circuits. The CPE is reduced to a resistance and ideal capacitive elements, when it is close to Zero and α = 1, respectively. The R, CPE and α extract parameters are summarized in **Table 1**. It is clear that the values of resistance R decrease with the increase in temperature, which is related to the increase of the mobility of charge carriers that was added to the conduction process **[41].**

The resistance at these temperature values can be deduced from the well-defined impedance peak, which was found to follow the Arrhenius relation:

$$R = R_0 \exp\left(\frac{E_{ac}}{k_B T} \right) \quad \textbf{(3)}$$

where R_0 is the pre-exponential term, and E_{ac} is the activation energy. The linear fitting, based on Eq. (3) shown in **Figure 6** as a straight line, yields the values of E_{ac} = 0.131, 0.194 and 0.143 eV for R_1, R_2, and R_3, respectively. It is therefore clear that the activation energy values obtained from both the Arrhenius plots of resistance and

frequency corresponding to the peaks of the imaginary part of impedance (Z"), in the same temperature region, are very close.

3) AC electrical conductivity:

Figure 7 displays the frequency dependence of the ac-conductivity of the prepared $Zn_{0,4}Ni_{0,6}Fe_2O_4$ spinel ferrite sample measured at different temperatures. One can see that the ac-conductivity spectra present two plateaus: one in low-frequency region with an independent frequency behavior for each temperature and the second one in the high-frequency region where the conductivity increases following the increase in the frequency. The origin of the frequency dependence of the conductivity can be attributed to the relaxation of the ionic atmosphere after the movement of the particle **[42].**

As mentioned before, three relaxations peaks were seen noticed in the imaginary part of the complex impedance. Accordingly, we can attribute the first plateau in the ac-conductivity to the contribution of boundary grains and electrodes contributions whereas the plateau at high frequencies is attributed to the grain contribution. To estimate the activation energy of the conduction process, we have calculated the conductivity of the grain, boundary grain, and electrode contributions, respectively (σ_1, σ_2 *and* σ_3) of our compound **(Table 2)** using:

$$\sigma_1 = \frac{e}{R_1 \times S} ; \sigma_2 = \frac{e}{R_2 \times S} ; \sigma_3 = \frac{e}{R_3 \times S} \quad (4)$$

where *e* is the thickness of pellet, *S* is its area and R_1, R_2 and R_3 are respectively the grain, boundary grain and electrode contributions resistance of the sample previously calculated from the intercept of the semicircular arc on real axis Z'.

In **Table 2**, we summarized the activation energy values. It is worth noting that the activation energy values obtained from both of conductivities (**Eq. 4**) and frequencies

corresponding to the peaks of the imaginary part of impedance (Z"), in the same temperature region, are very close. So, we can confirm the goodness of the fitting of the Nyquist plots.

~~In~~ **Figure 8** ~~we present~~ displays the temperature dependence of the ac-conductivity ($\log(\sigma_{ac}*T)$ *vs.* 1000/T). As shown, it linearly depends on the temperature and the adjustment of these curves, which allows us to calculate the activation energy values for different frequencies (inset of **Figure 8**). We note that the E_a decreases with the increase in frequency, which ~~confirm~~ proves that the applied field frequency enhances the electronic jumps between the localized states **[43].**

4) Magnetic properties:

Figure 9(a) represents the M *vs.* (μ_0H) curves of the $Zn_{0.4}Ni_{0.6}Fe_2O_4$ sample, collected at 5 K and at Room temperature with a maximum applied field of 10 T. At room temperature, the saturation magnetization (M_S) and the coercivity (H_C) of the $Zn_{0,4}Ni_{0,6}Fe_2O_4$ made by simple solid state reaction were found to be around 22 emu/g and 114 Oe, respectively. These are so close to the reported values of the same compound prepared ~~by different method~~ otherwise **[44-46]**. At both temperatures, ~~one can notice~~ an unsaturated magnetization was observed; it monotonically increases following the applied field and does not ~~attain~~ reach complete saturation even with maximum μ_0H field. Two necessary explanations could be used to explain this behavior; *(i)* the canted or disordered spins at the surface of the nanoparticles, which were difficult to align along the field direction causing an unsaturated magnetization in the sample, *(ii)* the presence of both ferromagnetic (FM) and the Antiferromagnetic (AFM) interaction processes in the compound.

A theoretical modulation of the M-H loops was used to separate out the ~~ferromagnetic~~ FM and the ~~antiferromagnetic~~ AFM contributions and to better understand the origin of the magnetization in the studied compound. We ~~have~~ used the following equation:

$$M(H) = 2\frac{M_{FM}^{S}}{\pi}\tan^{-1}\left\{\left(\frac{H \pm H_{ci}}{H_{ci}}\right)\tan\left(\frac{\pi \times M_{FM}^{R}}{2 \times M_{FM}^{S}}\right)\right\} + \chi H \quad (5)$$

where the first term is related to the ~~ferromagnetic~~ FM contributions and the second one represents the linear contribution from the ~~antiferromagnetic~~ ~~(~~AFM~~)~~ one [47, 48]. Here, M_{FM}^{S}, M_{FM}^{R}, H_{ci} are the ~~ferromagnetic~~ FM saturation magnetization, remnant magnetization, and intrinsic coercive field, respectively while χ is the ~~antiferromagnetic~~ AFM susceptibility. The fitted curves with both contributions are shown in **Figure 9(b).** The obtained parameters from the adjustment are listed in **Table 3**. It was noticed that the magnetization of the sample is principally due to the ~~ferromagnetic~~ FM contribution~~s~~ (~70% of the total magnetization) resulting in the ~~ferromagnetic~~ FM interactions between Iron ions.

IV. CONCLUSION:

In the present study, the $Zn_{0.4}Ni_{0.6}Fe_2O_4$ ferrite spinel was successfully synthesized via the standard solid-state reaction method at high temperature. In fact, the ~~X-Ray diffraction~~ XRD data have confirmed that its composition is single-phase with no detectable impurity and is crystallized in spinel structure. Additionally, the electrical study of this material ~~has shown~~ showed that the electrical properties are strongly dependent on both temperature and frequency. As for the complex impedance plots, they ~~have~~ revealed the presence of three semicircular arcs (grain, boundary grain, and electrode). Moreover, it has been established that as the temperature increases, the

area under the semicircles of the Nyquist plots decreases; thus proving the tendency of better conductivity of our ferrite sample. This behavior was modeled by an electrical equivalent circuit composed of three series sets of resistance and capacitance in parallel. The values of the activation energy calculated from conductivity and impedance are found to be very close, which confirms that the relaxation process and the conduction mechanism may be attributed to the same type of charge carriers. Finally, the magnetization hysteresis loops were analyzed by two contributions the ~~Antiferromagnetic~~ AFM and ~~Ferromagnetic~~ FM contributions and it was found that the magnetization is due essentially to the ~~ferromagnetic~~ FM contribution.

ACKNOWLEDGMENT

This work, within the framework of collaboration, is supported by the Tunisian Ministry of Higher Education and Scientific Research and the Portuguese Ministry of Higher Education and Scientific Research. Also, this work is funded by the FCT/MEC through national funds and when applicable co-funded by FEDER-PT2020 partnership agreement under the project, 5G-AHEAD IF/FCT-IF/01393/2015/CP1310/CT0002.

REFERENCES:

[1] A.C.F.M. Coasta, E. Tortella, M.R. Morelli, R.H.G.A. Kiminam, Synthesis, microstructure and magnetic properties of Ni–Zn ferrites, J. Magn. Magn. Mater. 256 (2003) 174–182.

[2] R.V. Mangalraja, S. Ananthakumar, P. Manohar, F.D. Gnanam, Dielectric behaviour of $Ni_{(1-x)}Zn_xFe_2O_4$ prepared by flash combustion technique, Mater. Lett. 57 (2003) 1151–1155.

[3] G. Rangamohan, D. Ravinder, A.V. Ramana Reddy, B.S. Boyanov, Dielectric properties of polycrystalline mixed nickel–zinc ferrites, Mater. Lett. 40 (1999) 39–45.

[4] M.U. Islam, T. Abbas, S.B. Niazi, Z. Ahmad, S. Sabeen, M.A. Chaudhry, Electrical behavior of fine particle, co-precipitation prepared Ni–Zn ferrites, Solid State Commun. 130 (2004) 353–356.

[5] A. Verma, T.C. Goel, R.G. Mediratta, R.G. Gupta, High resistivity nickel–zinc ferrites by the citrate precursor method, J. Magn. Magn. Mater. 192 (1999) 271–276.

[6] C. Upadhyay, D. Mishra, H.C. Verma, S. Anand, R.P. Das, Effect of preparation conditions on formation of nanophase Ni–Zn ferrites through hydrothermal technique, J. Magn. Magn. Mater. 260 (2003)188–194.

[7] E. Erdem, Electron beam curing of $CoFe_2O_4$ nanoparticles, Hybrid Materials, 1 (2014) 62-70.

[8] A. Verma, T.C. Goel, R.G. Mendiratta, M.I. Alam, Dielectric properties of NiZn ferrites prepared by the citrate precursor method, Mater. Sci. Eng. B, 60 (1999) 156–162.

[9] B.V. Bhise, M.B. Dongare, S.A. Patil, S.R. Sawant, X-ray infrared and magnetization studies on Mn substituted Ni-Zn ferrites, J. Mater. Sci. Lett. 10 (1991) 922–924.

[10] P.I. Slick, in: E.P. Wohlfarth (Ed.), Ferromagnetic Materials, North-Holland, Amsterdam 2 (1980) 196.

[11] T. Abraham, economics of ceramic magnets, Am. Ceram. Soc. Bull. 73 (1994) 62.

[12] Hulya Kaftelen, Mustafa Tuncer, Suyan Tu, Sergei Repp, Hasan Goçmez, Ralf Thomann, Stefan Weber, Emre Erdem, Mn-substituted spinel $Li_4Ti_5O_{12}$ materials studied by multifrequency EPR spectroscopy, J. Mater. Chem. A, 1 (2013) 9973–9982.

[13] Michael D. Drahus, Peter Jakes, Emre Erdem, Silke Schaab, Jun Chen, Mykhaylo Ozerov, Sergei Zvyagin, Rudiger-A. Eichel, Manganese-doped (1−x) $BiScO_3$–x$PbTiO_3$ high-temperature ferroelectrics: Defect structure and mechanism of enhanced electric resistivity, Physical Review B, 84 (2011) 064113.

[14] P. P. Hankare, U. B. Sankpal, R. P. Patil, I. S. Mulla, R. Sasikala, A. K. Tripathi, K. M. Garadkar, Synthesis and characterization of nanocrystalline zinc substituted nickel ferrites, J. Alloys Comp. 496(2010)256–260.

[15] R. Sharma, S. Singhal, Structural, magnetic and electrical properties of zinc doped nickel ferrite and their application in photo catalytic degradation of methylene blue, Physica B, 414 (2013) 83–90.

[16] N. Gupta, A.Verma, S.C. Kashyap, D.C. Dube, Dielectric behavior of spin deposited nanocrystalline nickel–zinc ferrite thin films processed by citrate-route, Sol. State Commun., 134 (2005) 689 –694.

[17] M. Ajmal, A. Maqsood, Influence of zinc substitution on structural and electrical properties of $Ni_{1-x}Zn_xFe_2O_4$ ferrites, Mat. Sci. Eng. B, 139 (2007)164–170.

[18] S.A. Uzma Ghazanfar, Siddiqi, G. Abbas, Study of room temperature dc resistivity in comparison with activation energy and drift mobility of NiZn ferrites, Mat. Sci. Eng. B118 (2005)132–134.

[19] M.U. Islam, T. Abbas, Shahida B. Niazi, Zubair Ahmad, Sadia Sabeen, M. Ashraf Chaudhry, Electrical behaviour of fine particle, co-precipitation prepared Ni–Zn ferrites, Solid State Commun.130(2004)353–356.

[20] S. Z. Cvejic, S. Rakic, S.J.Skuban, A. Kapor, Dielectric properties and conductivity of zinc ferrite and zinc ferrite doped with yttrium, J.Alloys Comp. 480(2009)241–245.

[21] S.S. Kumbhar, M.A. Mahadik, V.S. Mohite, K.Y. Rajpure, J.H. Kim, A.V. Moholkar, C.H. Bhosale, Structural, dielectric and magnetic properties of Ni substituted zinc ferrite, J. Magn. Magn. Mater., 363 (2014) 114–120.

[22] G. Umapathy, G. Senguttuvan, L. John Berchmans, V. Sivakumar, Structural, dielectric and AC conductivity studies of Zn substituted nickel ferrites prepared by combustion technique, J. Mater. Sci.: Mater. Electron, 27 (2016) 7062–7072.

[23] J.T.S. Irvine, A.R. West, E. Amano, A. Huanosta, R. Valenzuela, Characterisation of magnetic materials by impedance spectroscopy, Solid State Ionics 40-41 (1990) 220-223.

[24] G. Umapathy, G. Senguttuvan, L. John Berchmans, V. Sivakumar, Structural, dielectric and AC conductivity studies of Zn substituted nickel ferrites prepared by combustion technique, J. Mater. Sci.: Mater Electron, 27 (2016) 7062–7072.

[25] H.M. Rietveld, A profile refinement method for nuclear and magnetic structures, J. Appl. Crystallogr. 2 (1965) 65-71.

[26] A. Guinier, in: X. Dunod (Ed.), Théorie et Technique de la radiocristallographie, 3rd ed., 1964, p. 462.

[27] B. Ramesh, S. Ramesh, R. Vijaya Kumar, M. Lakshmipathi Rao, AC impedance studies on $LiFe_{5-x}Mn_xO_8$ ferrites, Journal of Alloys and Compounds 513 (2012) 289–293

[28] A. Benali, M. Bejar, E. Dhahri, M.F.P. Graça, L.C. Costa, Electrical conductivity and *ac* dielectric properties of $La_{0.8}Ca_{0.2-x}Pb_xFeO_3$ (x = 0.05, 0.10 and 0.15) perovskite compounds, J. Alloys Compd., 653 (2015) 506-512.

[29] F.Borsa, D.R. Torgeson, S.W.Martin, H.K. Patel, Relaxation and fluctuations in glassy fast-ion conductors: Wide-frequency-range NMR and conductivity measurements**,** Phys. Rev. B, 46 (1992) 795.

[30] F.S.H. Abu-Samaha, M.I.M. Ismail, AC conductivity of nanoparticles $Co_xFe_{(1-x)}Fe_2O_4$ (x=0, 0.25 and 1) ferrites, Materials Science in Semiconductor Processing, 19 (2014)50–56.

[31] E. Venkata Ramana, S.V. Suryana rayana, T. Bhima Sankaram, ac impedance studies on ferroelectromagnetic $SrBi_{5-x}La_xTi_4FeO_{18}$ ceramics, Mater. Res. Bull., 41 (2006) 1077-1088.

[32] N. Chihaoui, R. Dhahri, M. Bejar , E. Dharhi, L.C. Costa, M.P.F. Graça, Electrical and dielectric properties of the $Ca_2MnO_{4-\delta}$ system**,** Solid State Communications 151 (2011) 1331–1335**.**

[33] Y. Purushotham, M.B. Reddy, Pran Kishan, D.R. Sagar and P. Venugopal Reddy, Electrical conductivity and thermopower studies of titanium-substituted lithium-magnesium ferrites, Materials Letters 17 (1993) 341-345.

[34] S. A. Mazen, Electrical Conductivity and Thermoelectric Power of Cu-Ti Ferrite, Materials Chemistry and Physics 56, (1998) 102-107.

[35] H. Rahmouni, A. Benali, B. Cherif, E. Dhahri, M. Boukhobza, K. Khirouni, M. Sajieddine, Structural and electrical properties of $Zn_{1-x}Ni_xFe_2O_4$ ferrite, Physica B: Condensed Matter, 466–467, (2015) 31-37.

[36] A. Kumar, N.M. Murari, R.S. Katiyar, Investigation of dielectric and electrical behavior in $Pb(Fe_{0.66}W_{0.33})_{0.50}Ti_{0.50}O_3$ thin films by impedance spectroscopy J. Alloys Compd. 469 (2009) 433.

[37] E. Barsoukov, J. Ross Macdonald, Impedance Spectroscopy Theory, Experiment and Applications, second ed., Wiley Interscience, New York (2005) 14.

[38] U. Intatha, S. Eitssayeam, J. Wang, T. Tunkasiri, Impedance study of giant dielectric permittivity in $BaFe_{0.5}Nb_{0.5}O_3$ perovskite ceramic, Curr. Appl. Phys. 10 (2010) 21.

[39] A. Omri, M. Bejar, E. Dhahri, M. Es-Souni, M.A. Valente, M.P.F. Graça c, L.C. Costa, Electrical conductivity and dielectric analysis of $La_{0.75}(Ca,Sr)_{0.25}Mn_{0.85}Ga_{0.15}O_3$ perovskite compound, J. Alloys Compd., 536 (2012) 173–178

[40] O. Bohnke, J. Emery, J.L. Fourquet, Anomalies in Li^+ ion dynamics observed by impedance spectroscopy and ^7Li NMR in the perovskite fast ion conductor $(Li_{3x}La_{2/3-x}{}_{1/3-2x})TiO_3$, Solid State Ionics. 158 (2003) 119.

[41] N. Elghoul, M. Wali, S. Kraiema, H. Rahmouni, E. Dhahri, K. Khirouni, Sodium deficiency effect on the transport properties of $La_{0.8}Na_{0.2-x}\square_xMnO_3$ manganites, Physica B 478(2015)108–112

[42] E. Barsoukov, J. Ross Macdonald, Impedance Spectroscopy Theory, Experiment and Applications, second ed., Wiley Interscience, New York, 2005, 14.

[43] M. Okutan, E. Basaran, H.I. Bakan, F. Yakuphanoglu, The dielectric spectroscopy and surface morphology studies in a new conjugated polymer poly(benzobisoxazole-2,6-diylvinylene), J. Phys. B 364 (2005) 300.

[44] S.B. Waje, M. Hashim, W.D.W. Yusoff, Z. Abbas, Sintering temperature dependence of room temperature magnetic and dielectric properties of

$Co_{0.5}Zn_{0.5}Fe_2O_4$ prepared using mechanically alloyed nanoparticles, J. Magn. Magn. Mater. 322 (2010) 686–691

[45] M. Penchal Reddy, G. Balakrishnaiah, W. Madhuri, M. Venkata Ramana, N. Ramamanohar Reddy, K.V. Siva Kumar, V.R.K. Murthy, R. Ramakrishna Reddy, Structural, magnetic and electrical properties of NiCuZn ferrites prepared by microwave sintering method suitable for MLCI applications, J. Phys. Chem Solids 71 (2010) 1373–1380.

[46] H. Bahiraei, M.Z. Shoushtari, K. Gheisari, C.K. Ong, The effect of sintering temperature on the electromagnetic properties of nanocrystalline MgCuZn ferrite prepared by sol–gel auto combustion method, Mater. Lett. 122 (2014) 129–132.

[47] L. R. Shah, H. Zhu,W. G. Wang, B. Ali, T. Zhu, X. Fan, Y. Q.Song, Q. Y. Wen, H. W. Zhang, S. I. Shah, and J. Q. Xiao, Effect of Zn interstitials on the magnetic and transport properties of bulk Co-doped ZnO, J. Phys. D: Appl. Phys., 2010, 43, 035002.

[48] P. Kumar, N. Shankhwar, A. Srinivasan, and M. Kar, Oxygen octahedra distortion induced structural and magnetic phase transitions in $Bi_{1-x}Ca_xFe_{1-x}Mn_xO_3$ ceramics, J. Appl. Phys., 2015, 117, 194103.

Figure Captions

Figure 1: Observed (open symbols) and calculated (solid lines) X-ray diffraction pattern for $Zn_{0.4}Ni_{0.6}Fe_2O_4$ compound. Positions for the Bragg reflections are marked by vertical bars. Differences between the observed and the calculated intensities are shown at the bottom of the figure.

Figure 2: (a) Top view of the surface morphologies of $Zn_{0.4}Ni_{0.6}Fe_2O_4$ sample obtained by SEM technique, **(b)** EDAX spectra, **(c)** Lorentzian distribution of particle sizes.

Figure 3: Variation of real part of the impedance (Z') of the $Zn_{0.4}Ni_{0.6}Fe_2O_4$ compound as a function of frequency for different temperatures. **The inset** shows the scaling behavior of Z' at 480K.

Figure 4: (a) Variation of imaginary part of the impedance (Z") of the $Zn_{0.4}Ni_{0.6}Fe_2O_4$ compound as a function of frequency for different temperatures, **(b)** The Arrhenius plots for $Zn_{0.4}Ni_{0.6}Fe_2O_4$ compound logarithm of frequency vs.1/T.

Figure 5: Cole–Cole plots of $Zn_{0.4}Ni_{0.6}Fe_2O_4$ compound at several temperatures. **Insert:** the equivalent circuit formed by a series of three parallel combination of resistance (R) and Constant Phase Element Impedance (Z_{CPE}) (R-CPE circuit).

Figure 6: The Arrhenius plots for $Zn_{0.4}Ni_{0.6}Fe_2O_4$ compound logarithm of resistances vs. 1/T.

Figure 7: Frequency dependence of the ac conductivity at various temperatures of the $Zn_{0.4}Ni_{0.6}Fe_2O_4$ compound.

Figure 8: the temperature dependence of the ac conductivity. The inset shows the activation energy values as function of frequency.

Figure 9: (a) Magnetization versus magnetic field (M-H) curves for $Zn_{0.4}Ni_{0.6}Fe_2O_4$ compound, **(b)** Antiferromagnetic and Ferromagnetic Fitted Magnetization versus magnetic field (M-H) curve at room temperature for $Zn_{0.4}Ni_{0.6}Fe_2O_4$.

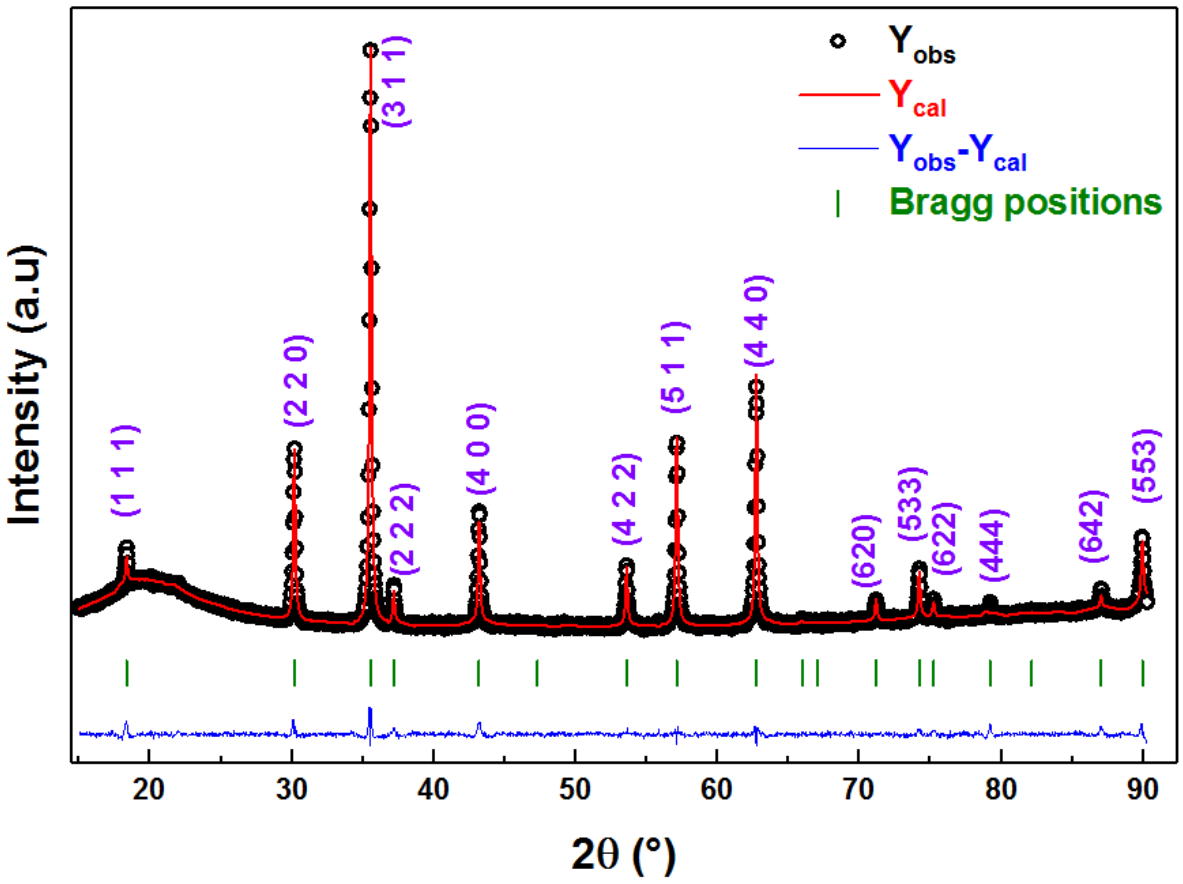

Figure 1:

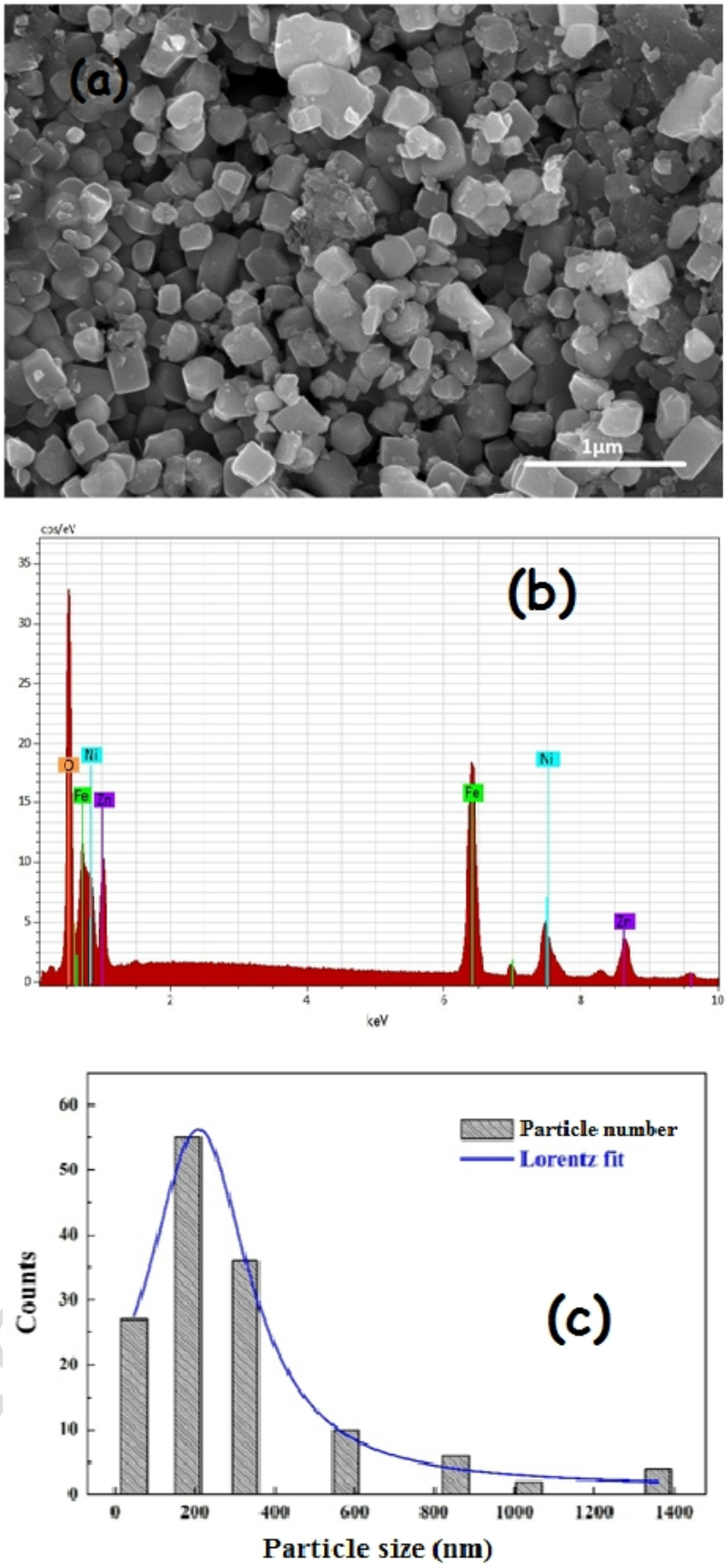
(a)
1μm
cps/eV
(b)
O
Ni
Fe
Zn
Fe
Ni
Zn
keV
Particle number
Lorentz fit
(c)
Counts
Particle size (nm)

Figure 2:

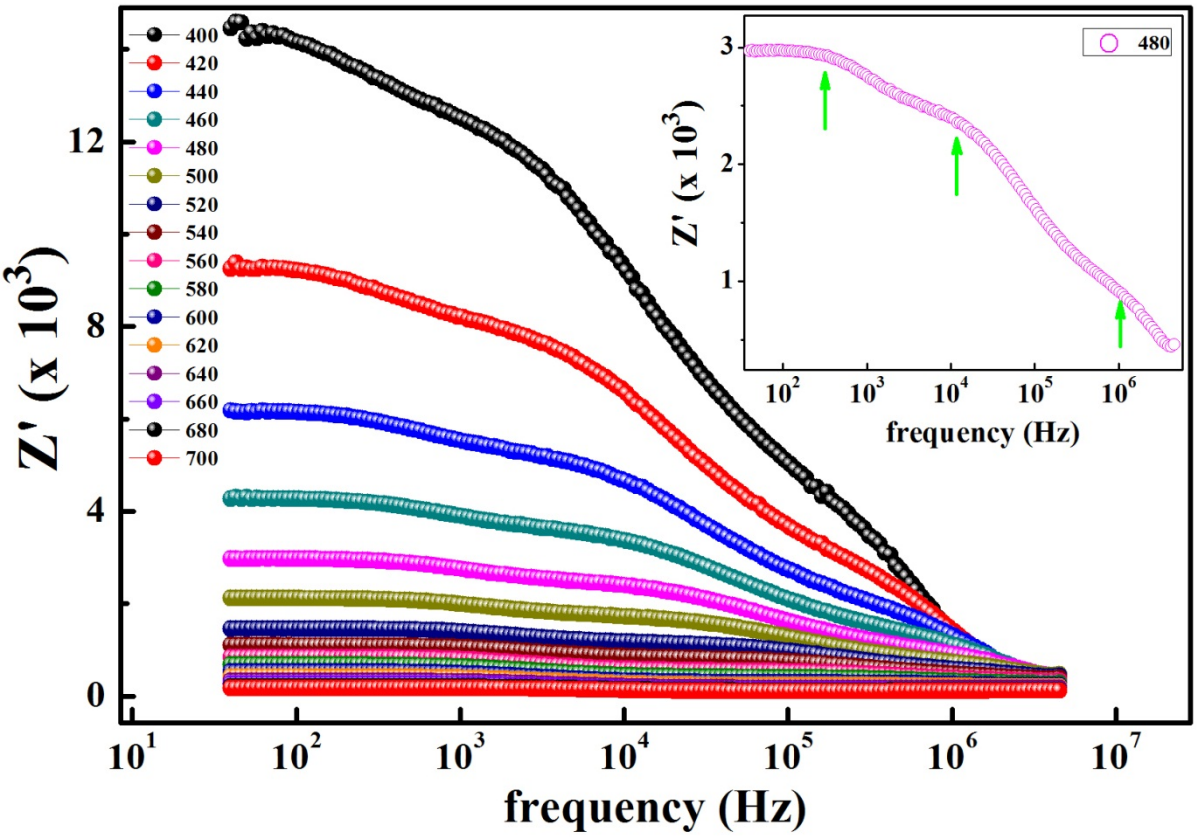

Figure 3:

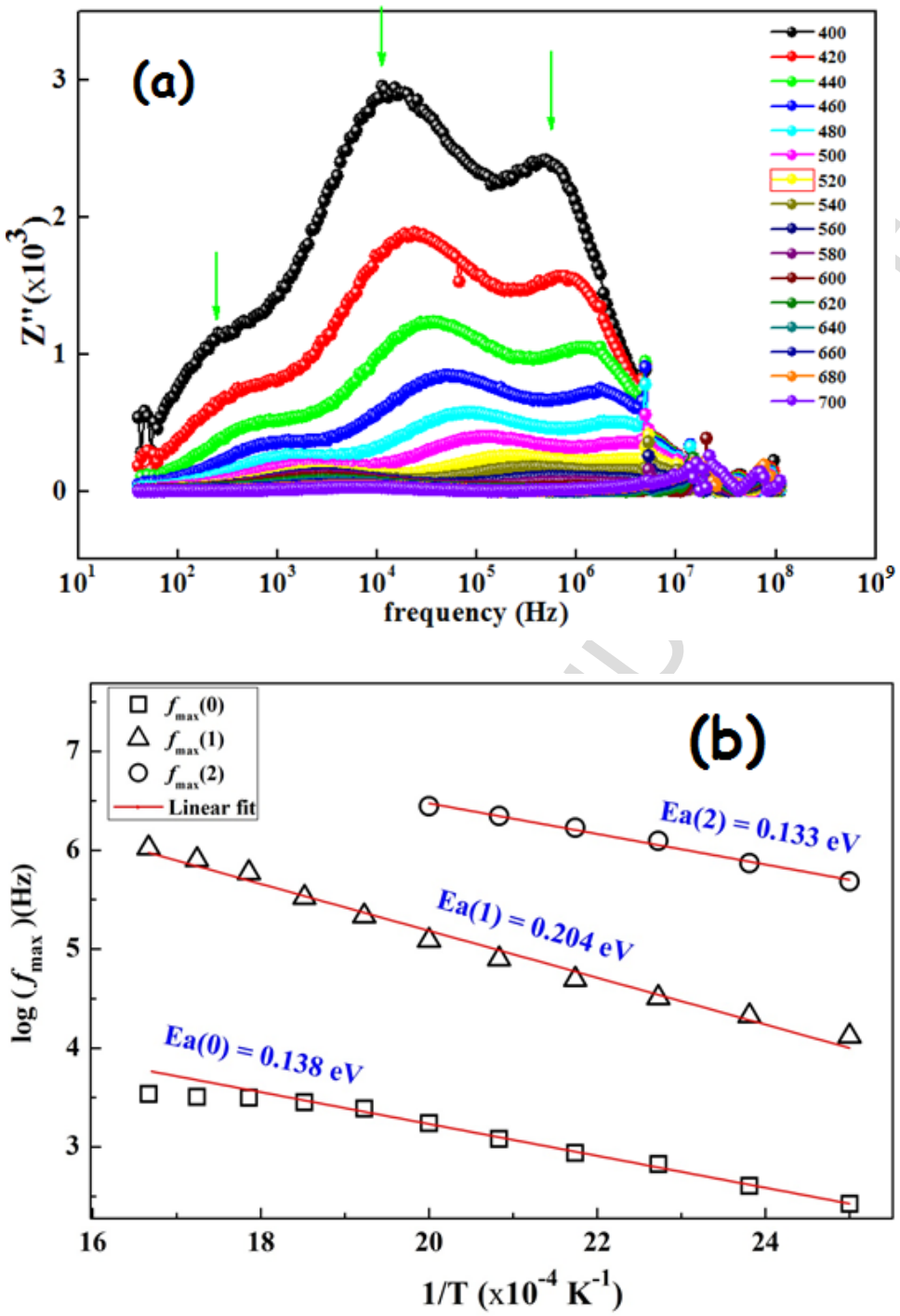
(a)
Z''(x10^3)
frequency (Hz)
400
420
440
460
480
500
520
540
560
580
600
620
640
660
680
700
(b)
f_max(0)
f_max(1)
f_max(2)
Linear fit
Ea(2) = 0.133 eV
Ea(1) = 0.204 eV
Ea(0) = 0.138 eV
log (f_max)(Hz)
1/T (x10^-4 K^-1)

Figure 4:

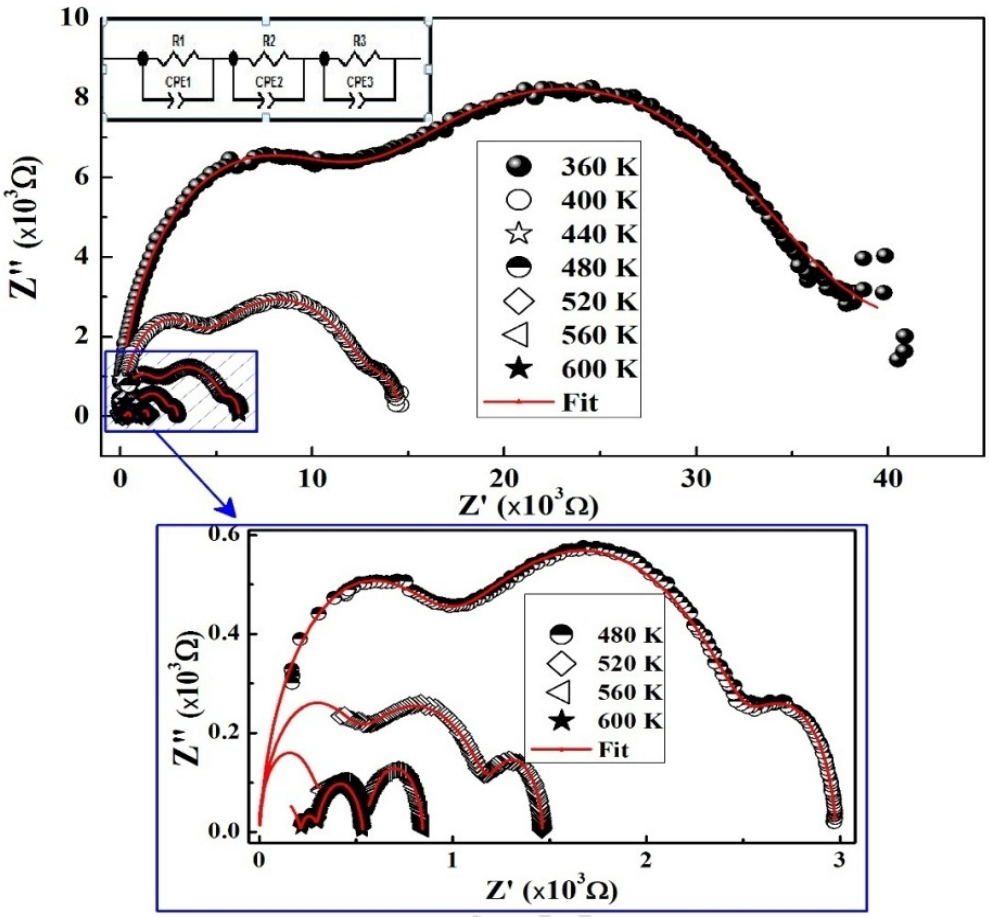

Figure 5:

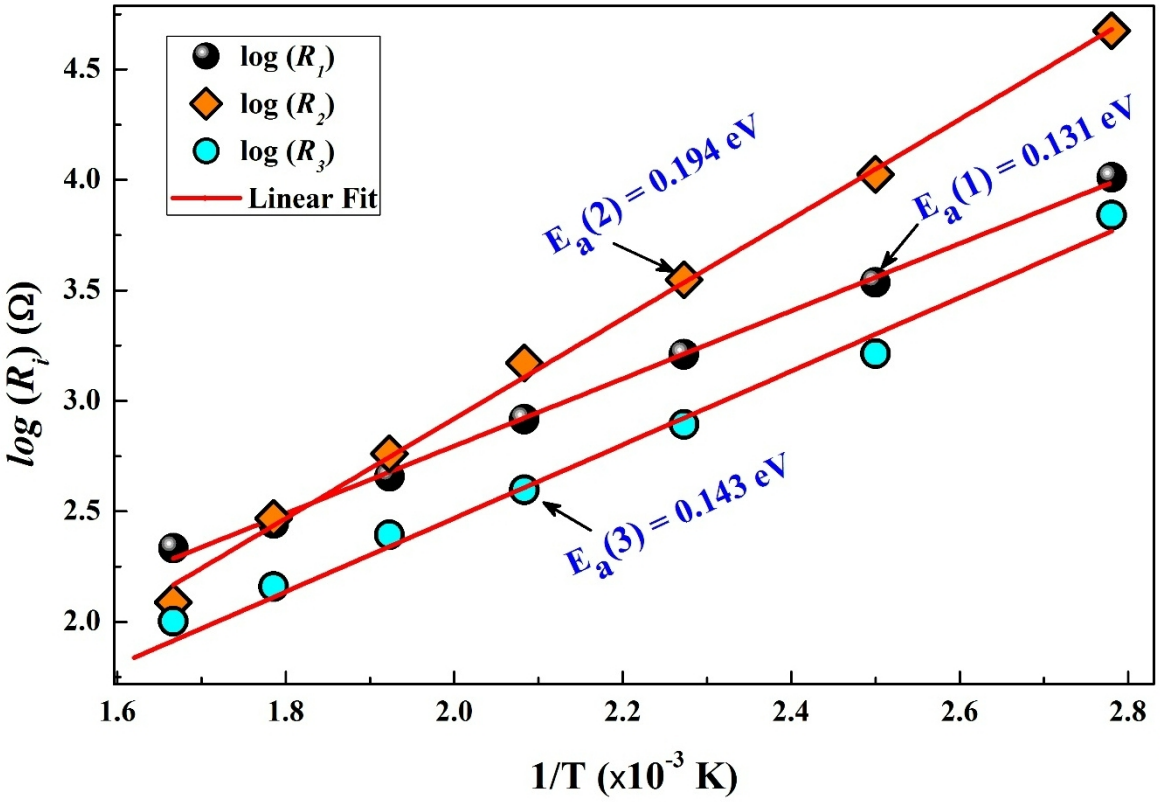

Figure 6:

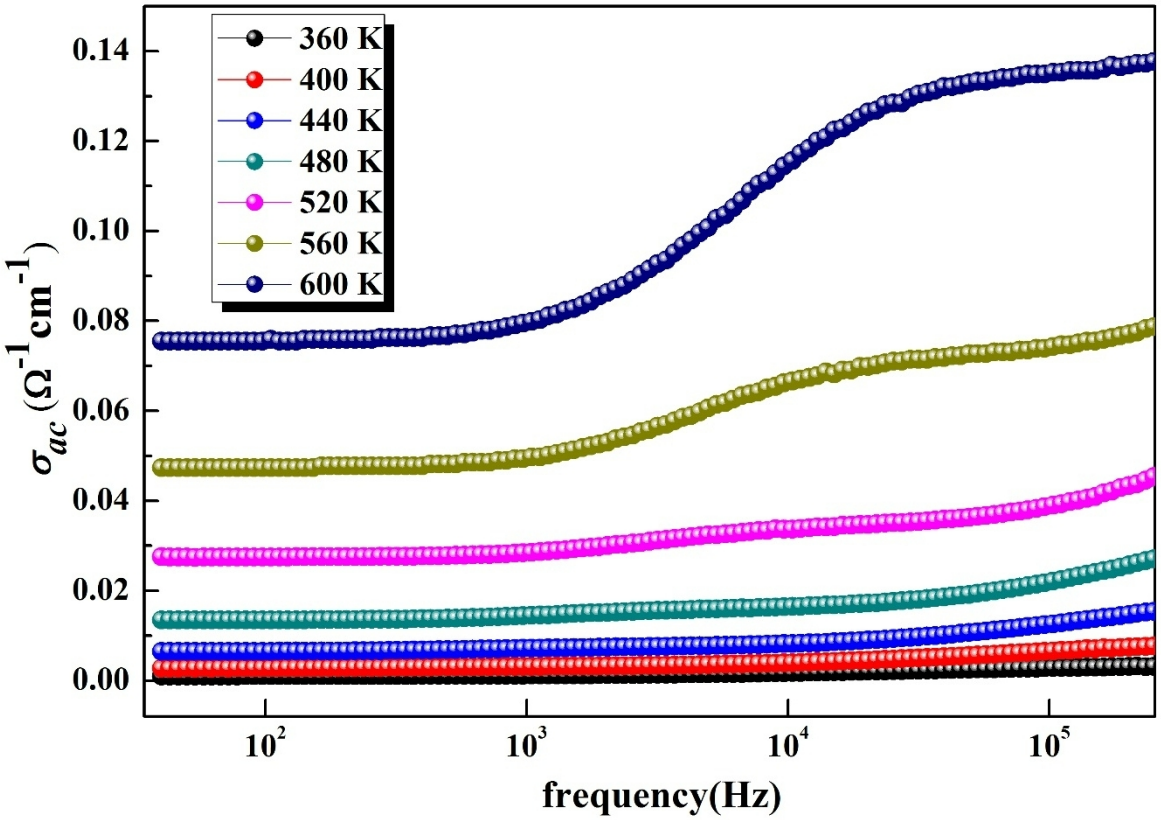

Figure 7:

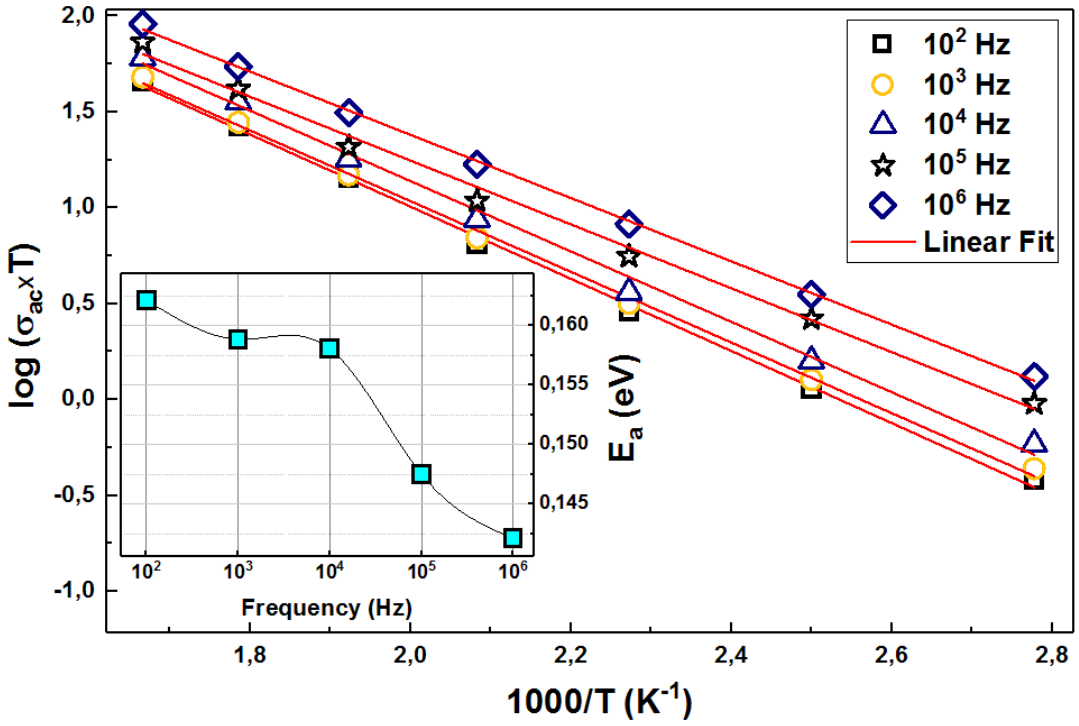

Figure 8:

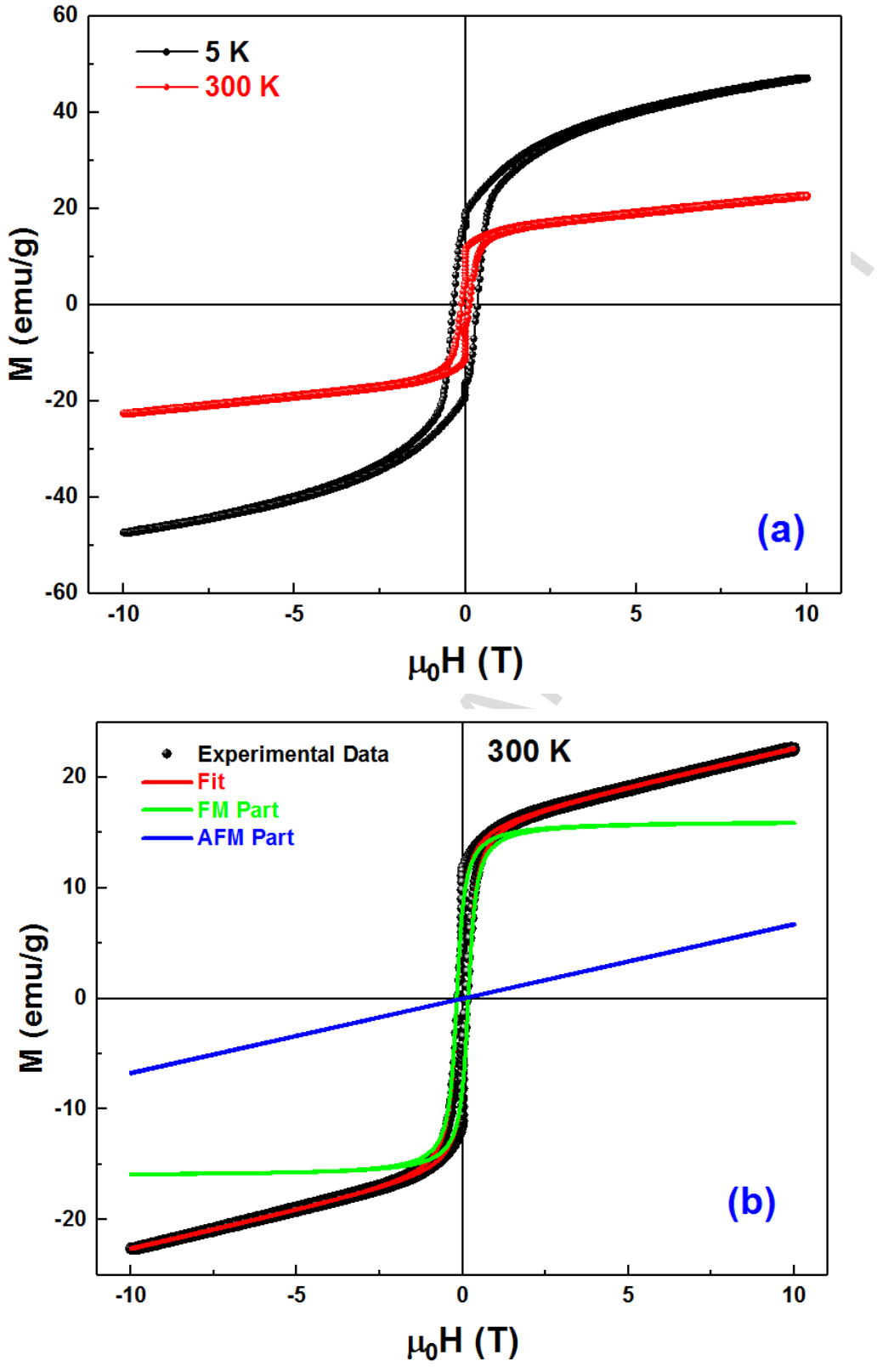
5 K
300 K
M (emu/g)
μ0H (T)
(a)
Experimental Data
Fit
FM Part
AFM Part
300 K
M (emu/g)
μ0H (T)
(b)

Figure 9

Research Highlights

- The complex impedance plots have revealed the presence of three semicircular arcs.
- Values of the activation energy calculated from σ_{ac} and Z" are very close.
- The electrical properties are strongly dependent on both temperature and frequency.
- The applied field frequency enhances the electronic jumps between the localized states.
- The ferromagnetic contribution presents 70% of the total magnetization.

Table 1: values of the electrical parameters deduced from the complex diagram for $Zn_{0.4}Ni_{0.6}Fe_2O_4$ compound at several temperatures.

T(K)	$R_1(\Omega)$	C_1 (10^{-11} F)	α_1	$R_2(\Omega)$	C_2 (10^{-8} F)	α_2	$R_3(\Omega)$	C_3 (10^{-7} F)	α_3
360	10272	7.405	0.994	39345	3.327	0.682	6918	44.570	0.725
400	3431	5.896	1.001	9945	5.297	0.658	1635	12.241	0.90
440	1624	9.362	0.977	4000	5.802	0.679	783	4.466	1.034
480	826.6	11.71	0.957	1788	6.237	0.691	396	4.732	0.992
520	455.2	9.834	0.950	760	5.687	0.710	247.9	3.702	0.986
560	278.8	10.72	1.008	293.4	4.514	0.739	144.5	3.959	0.938
600	215.6	11.65	0.696	84.58	3.692	0.802	100.7	7.627	0.877

Table 2: the resistance, the conductivity and the activation energy of the grain, boundary grain and electrode for $Zn_{0.4}Ni_{0.6}Fe_2O_4$ compound

T(K)	$R_1(\Omega)$	$\sigma_1(\Omega^{-1}cm^{-1})$	E_a(eV)	$R_2(\Omega)$	$\sigma_2(\Omega^{-1}cm^{-1})$	E_a(eV)	$R_3(\Omega)$	$\sigma_3(\Omega^{-1}cm^{-1})$	E_a (eV)
360	10272	0.00391		39345	0.00102		6918	0.0058	
400	3431	0.0117		9945	0.00404		1635	0.02456	
440	1624	0.02472		4000	0.01004		783	0.05128	
480	826.6	0.04857	**0.131**	1788	0.02246	**0.194**	396	0.10139	**0.143**
520	455.2	0.0882		760	0.05283		247.9	0.16196	
560	278.8	0.14401		293.4	0.13684		144.5	0.27785	
600	215.6	0.18622		84.58	0.4747		100.7	0.39871	

Table 3: Parameters extracted from fitting the magnetization hysteresis loops of $Zn_{0.4}Ni_{0.6}Fe_2O_4$ compound

Paramagnetic contribution	Ferromagnetic contribution		
χ (10^{-5} emu/g*gauss)	H_{CI} (Gauss)	M_{FM}^{S} (emu/g)	M_{FM}^{R} (emu/g)
6.761	1752	14.257	7.671